ASM Handbook, Volume 11, *Failure Analysis and Prevention*
B. Miller, R. Shipley, R. Parrington, D. Dennies, editors
DOI 10.31399/asm.hb.v11.a0006793

Impact Wear Failures

Roger Lewis, Mohanad Zalzalah, and Tom Slatter, The University of Sheffield

IMPACT OR PERCUSSIVE WEAR has been defined as "the wear of a solid surface that is due to percussion, which is a repetitive exposure to dynamic contact by another body" (Ref 1). This is a restricted definition ignoring erosive wear by impact of streams of small particles, which is covered elsewhere in this Volume. Impact wear, however, has many analogies to the field of erosive wear. The main difference is that in impact wear situations, the bodies tend to be large and contact in a well-defined location in a controlled way, unlike erosion where the eroding particles are small and interact randomly with the target surface.

There are many industrial situations in which impacting bodies are employed where failures due to wear can be costly and safety, reliability, and quality can be greatly reduced.

Excessive wear from inlet and exhaust valves impacting their seating faces in automotive engines can lead to loss of cylinder pressure and ultimately engine failure. Failure of tools used for drilling rock and other media raises cost concerns associated not only with the need for frequent replacement of parts but also in the downtime incurred. Unintentional impacts, such as those arising from the chattering and relative motion of tubes carrying waste from nuclear reactors, can give rise to situations where safety and reliability are of critical concern. Potential impact wear problems are also found in dental implants and heart valves, where health and well-being are at stake.

In this article, some generic features of impact wear are described and two particular examples are examined in detail.

Impact Wear Modes

Two modes of impact wear are apparent (Fig. 1). When the relative approach of the bodies contains no tangential or rotational elements, it is described as normal-impact wear. Where a shear component is added, either when normal impact occurs with a component of sliding or the bodies impact at a tangent, it is termed compound-impact wear. Most of the situations described previously involve impact with a small amount of sliding. Compound-impact wear has been shown to lead to much higher wear rates than normal impact alone (Ref 2, 3). This is thought to be due to enhanced removal of wear debris that occurs with the introduction of a shear component.

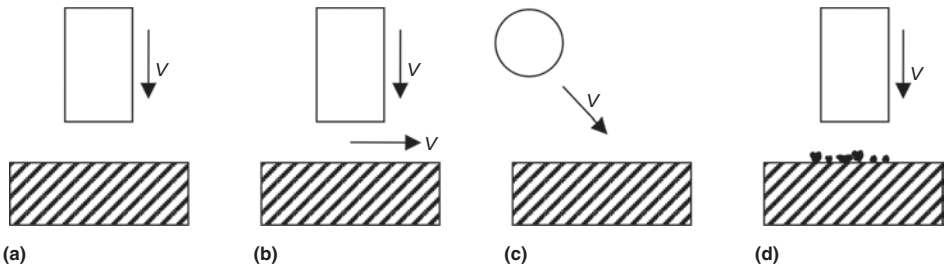

Fig. 1 Schematic diagram of impact wear modes resulting from bodies variously moving with velocity, *V*. (a) Normal impact. (b) Compound impact (with motion of both bodies causing sliding on impact). (c) Compound impact (with tangential contact causing sliding on impact). (d) Normal impact with a third body

When one body impacts a second at different positions, one-body wear will occur, for example, a printer typeface that is repeatedly impacted against continually renewed paper. In situations where a body repetitively impacts at the same position, for example, in devices such as solenoid valves, it is likely that both will experience surface degradation and two-body wear will occur. However, if one of the surfaces is more prone to wear than the other, it may still result in one-body wear.

Another situation that must be considered is the presence of a third-body material. This may be in the form of a lubricant applied to help mitigate a wear or friction problem (Ref 4), or in the form of wear debris, or something there naturally as part of the operating environment, such as sand (Ref 5, 6).

Impact Wear of Metals

Deformation during Impact

In bodies subjected to repetitive impulse loading, characteristic subsurface zones have been observed for a large variety of materials under various test conditions (with both normal and compound impact) (Ref 7).

In general, three subsurface regions can be seen, as shown schematically in Fig. 2. The first, furthest from the contact surface, consists of undisturbed base material. The deformation zone, the intermediate region, consists of plastically deformed base material. The deformation ranges from zero at the interface with zone 1 to a maximum at the interface with the third region, the white layer. The white layer, containing the contact surface, is usually homogeneous and finely structured.

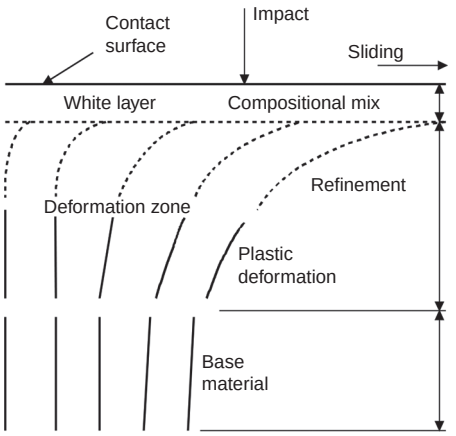

Fig. 2 Schematic representation of subsurface zones found beneath surfaces subjected to repetitive impact loading. Source: Ref 7

The characteristics of the subsurface regions vary with the impacting materials and the conditions of stress and sliding speed at the contact. In some cases, there is strong evidence of crack and void formation in subsurface

regions (Ref 8), while in others, no cracks are visible (Ref 9). In other specimens, varying degrees of crack formation in the white layer or along the deformation zone/white layer interface have been observed (Ref 10).

The composition of the white layer is often mixed, consisting of material from both impacting bodies as well as constituents of the operating environment. In one-body wear situations, the white layer in one body can be entirely made up of material transferred from the second body.

Subsurface regions form on both impacting bodies and grow very quickly, within a few hundred impacts (Ref 11). Once formed, the white layer and the deformation zone maintain a steady-state configuration as more impacts occur.

The formation of the white layer has been attributed to adhesion (Ref 12), although mechanical "mixing" and diffusion also take place. More probably, a combination of these three occurs to give the specific morphology and composition of the white layer. The deformation zone is clearly formed by the repetitive stress cycling.

The hardness of the material forming the surfaces of the impacting bodies has been noted to increase (Ref 2, 8, 12). Within the deformation zone, this is credited to work hardening, whereas in the white layer, it is a property of the near-surface material developed in situ (Ref 12).

A different subsurface region system develops when a brittle or nondeforming matrix is subjected to repetitive impact (Ref 12). A white layer still forms, but the base material tends to remain undeformed (Fig. 3).

Material-Removal Mechanisms

The mechanisms by which material can be removed from a surface by repeated impacts include the following (Ref 5, 6, 13):

- *Oxidative wear:* mild wear regime, where contacting bodies are separated by oxide films, thus reducing metal-to-metal contact
- *Adhesion:* a more severe wear regime characterized by material smearing and transfer
- *Abrasion:* equally severe, one-, two-, or three-body modes lead to the formation of plowing grooves
- *Surface fatigue:* more severe wear again, leading to subsurface crack nucleation and subsequent delamination or spalling of surface material
- *Plastic deformation:* while not leading to actual material removal, causes displacement of material from the contact area through "mushrooming"

Several of these mechanisms of impact wear are shown in Fig. 4. Figure 5 also illustrates how plastic flow may occur in the counterface, where shoulders can form of material removed from the contact zone that is no longer load bearing but would not be measured as lost mass.

The mechanisms occurring in a given impact case are determined by the stress and sliding conditions within the contact. For example, in high-strength tungsten carbide bits of rock-drilling equipment, surface fatigue leads to the formation of spalls (Ref 15). Repetitive impact of metallic components at low stress levels, however, is more likely to result in small, submicrometer wear particles and a highly oxidized surface state.

It has been shown that under moderate conditions of normal or compound impact, wear is caused by a process similar to that of adhesive wear during sliding (Ref 3, 16). More severe conditions at the contact lead to the occurrence of surface fatigue, subsurface crack growth, and spalling (Ref 15, 17–19). Very large impact energies bring about failures due to surface fracture and produce rapid material removal (Ref 20, 21). This evolution of wear mechanisms as the conditions in an impact contact become more severe is illustrated in Fig. 6.

Oxidative Wear

Oxidative wear tends to occur at low stress levels and can be found in both normal and compound-impact contacts. Wear rates are low because the contacting surfaces are separated by oxide films, which tend to have better lubricating properties than bare metal surfaces. Wear debris is generally fine and predominantly made up of metal oxide. Oxidative wear is particularly prevalent in contacts with a small amount of sliding or those in which fretting occurs, such as the backprinter device of a hammer striking against a print band (Ref 22).

Adhesive Wear

Adhesive wear occurs in both compound and normal-impact contacts; it is characterized by material smearing and transfer of material from one contacting body to the other (Ref 23). This occurs as a result of the formation of welded junctions at asperity tips, as shown in Fig. 7. Cracks nucleate in the work-hardened tips that break away while remaining adhered to the lower surface. This can occur as one-body wear, when material is only transferred from one body, or as two-body wear, when it occurs from both.

Abrasive Wear

Abrasive wear, mainly found in compound-impact contacts, manifests itself as plowing

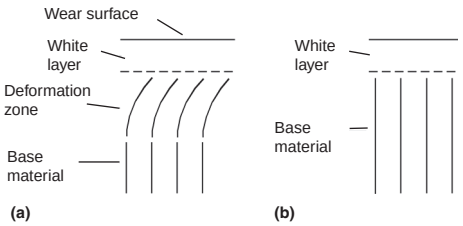

Fig. 3 Subsurface regions for (a) ductile and (b) brittle or nondeforming materials

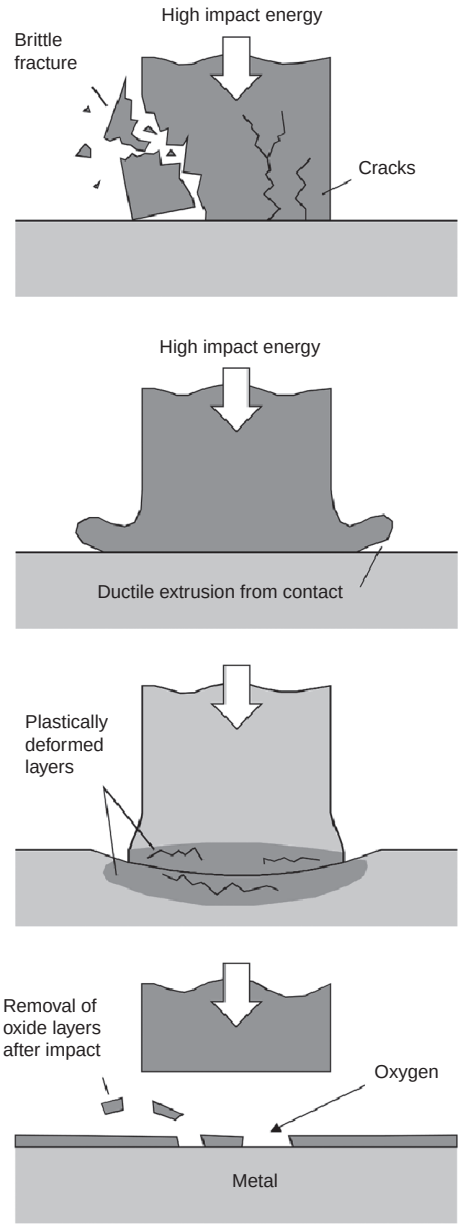

Fig. 4 Schematic diagrams of the different mechanisms of impact wear. Source: Ref 14

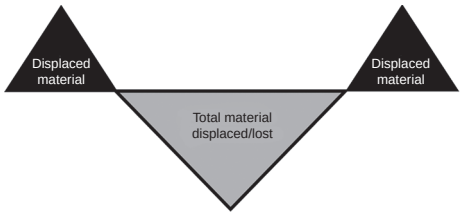

Fig. 5 Model of lost versus displaced counterface material

grooves and leads to a roughening of the contact surface (Ref 24). The grooves become more accentuated as impact stresses increase. However, under closer examination, it can be seen that at higher impact stresses, there is evidence of crack nucleation and the formation of flat, platelike particles within the grooves (Ref 8). Inclusion of another material in the interface, such as sand, will also promote abrasive wear in compound impacts (Ref 5, 6).

Surface Fatigue and Delamination

In general, impact wear failure mechanisms are dependent on the formation of the subsurface layers described in the previous section. Fatigue failure in impact is mainly induced in the white layer—the subsurface zone including the wear surface (Fig. 2) (Ref 11, 12, 25, 26).

Two mechanisms have been identified within the white layer that explain the occurrence of delamination and spalling of impacting bodies, respectively (Ref 25), as shown in Fig. 8.

In the case of impacting bodies, the white layer builds up on the wear surface as impacts progress and becomes intensely work hardened. As a result, microcracks are easily nucleated within the white layer material (Fig. 8a). The path of least resistance along which the cracks can propagate is the deformation zone/white layer interface, and hence, it is here that delamination occurs (Fig. 8b).

This process is thought to be different than the conventional delamination theory (Ref 27, 28), in which increasing shear deformation, as a result of bodies sliding against one another under load, leads to the piling up of subsurface dislocations. These cause the nucleation of microcracks, which subsequently lead to the occurrence of delamination.

As well as the surface white layer, white layers have been observed subsurface at depths of tens to several hundred micrometers in bodies subjected to repetitive impacts (Ref 26). Propagation of cracks in a subsurface white layer will lead to removal of material between the wear surface and the white layer.

Spalling occurs when microcracks within the white layer propagate in a direction perpendicular to the wear surface and parallel to the flow lines in the deformation zone (Fig. 8c). The direction of the crack propagation is affected by defects present in the deformation zone. Microcracks in the white layer tend to merge with cracks formed at defects in the deformation zone.

Figure 9 shows an example of this type of delamination. The image was taken from the impact crater of EN8 steel tested at 60° impact.

Plastic Deformation

While mass loss in impact wear mainly results from wear debris arising from the subsurface zones, wear also occurs as a result of plastic deformation and subsequent "mushrooming" of the impacting bodies, leading to the creation of leading and trailing edges (Fig. 4) (Ref 8, 9, 14).

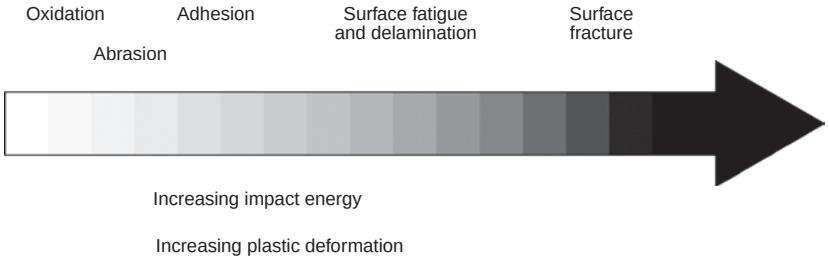

Fig. 6 Evolution of impact wear mechanisms as conditions in a contact become more severe

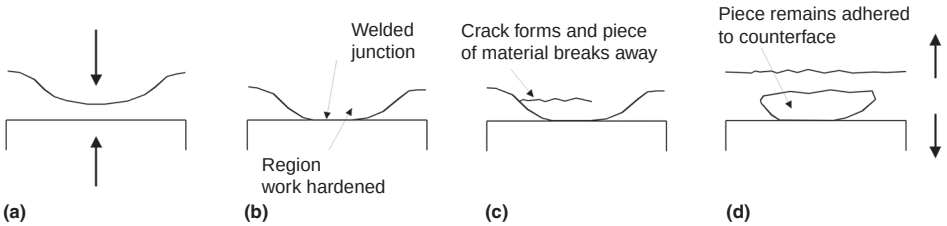

Fig. 7 Schematic diagram of the formation of an adhesive transfer particle. (a) Bodies contact. (b) Welded junction forms. (c) Cracks initiate and material breaks away. (d) Debris from one body adheres to the other.

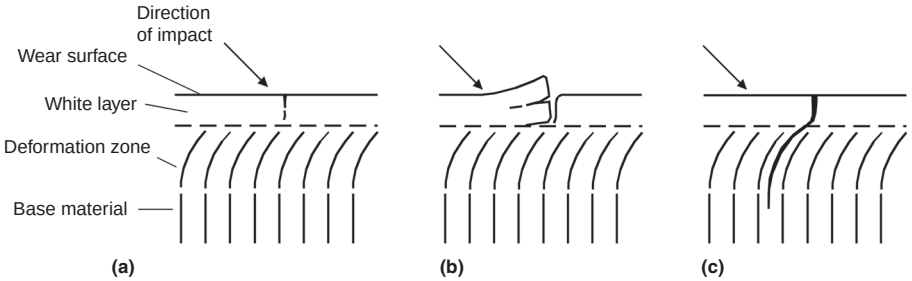

Fig. 8 Failure mechanisms induced by the white layer. Source: Ref 25

Influences on Wear

Contact Stress

One of the largest influences on normal- and compound-impact wear failures is contact stress (Ref 12). At low impact stresses, there is some evidence of local fracture and deformation. At significantly higher stresses, greater deformation occurs and a distinct deformation zone is formed. Wear rates increase with increasing contact stress, as shown in Fig. 10 (Ref 8). The data are plotted as change in specimen height rather than mass loss, because impact stress was varied by altering the contact area; therefore, the larger-diameter specimens would have lost more mass.

It should be noted that contact stress during a test can be quite large. Fricke and Allen (Ref 29) observed that the contact area for a line contact at 5 J (3.7 ft · lbf) impact energy was 4 times higher after 100,000 cycles than at the start of the test. This must be thought out when considering the wear trends observed with increasing cycles.

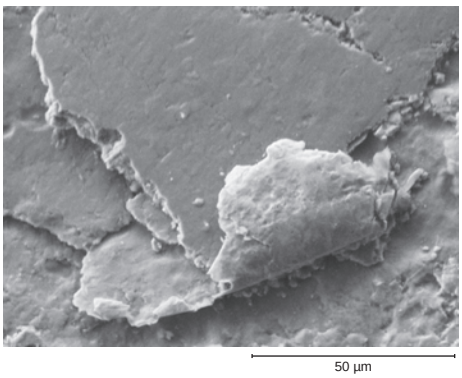

Fig. 9 Delamination wear of EN8 steel in a 60° impact

In more recent work on impact wear, impact energy is quoted rather than contact stress. However, the trends seen are similar to those shown in Ref 29 and 30.

Sliding Velocity

The other main influence is sliding velocity (Ref 11). In bodies impacted with a low sliding velocity, crack formation occurs. At higher velocities, however, the white layer is usually quite homogeneous and integrally bonded to its substrate. These two mechanisms lead to observations that wear rates both increase and decrease with increasing sliding velocity (Fig. 11, 12) (Ref 8, 31). This can be explained by studying data over a greater range of sliding velocities, as shown in Fig. 13 (Ref 23). As can be seen, the wear exhibits both a maximum and a minimum over the range of sliding velocities tested. This phenomenon has also been observed in high-speed sliding wear tests (Ref 32).

Specimen Stiffness

Specimen stiffness affects the wear rate of both impacting bodies (Ref 24). As shown in Fig. 14, the short, stiff specimen (an ultrahigh-strength steel) wore the counterface (a stainless steel) and yet hardly wore at all itself. In contrast, the longer and less stiff specimen wore considerably more, yet its counterface was worn much less than that with the stiffer specimen.

Hardness

Microstructure and bulk material hardness also play a role in impact wear (Ref 8, 33). These are critical in determining the development of the white layer and the subsequent crack nucleation and wear debris formation.

Work has shown that treatment of materials such as cast iron or stainless steel via techniques such as laser hardening (Ref 34, 35), induction hardening (Ref 36), and cryogenic processing (Ref 37) improved wear resistance considerably over untreated material. However, care must be taken to control the processing so as not to cause embrittlement and possibly introduce cracking on impact application.

Work hardening during impacts is also an important factor. Some materials work harden more than others (Ref 29), so bulk hardness is not always the best indicator of possible wear behavior.

Lubrication

In repetitive normal-impact applications with lubrication, it is probable that asperity contact will be frequent, except for combinations of low-contact-pressure, high-viscosity oils and low surface roughness. It is likely, therefore, that the contact will be boundary lubricated, in which case the surface shear stresses will not differ substantially from the dry case. Thus, a boundary-lubricated, normal-impact contact is essentially quasi-dry. Wear is therefore not likely to be reduced with lubrication of a normal contact.

In an oil-lubricated compound-impact contact, due to the tendency for a full film to form, a superimposed sliding speed is conducive to less wear. This is in contrast to dry impact, where introducing sliding substantially increases wear. Lubrication tends to reduce sliding friction so that even if a full film does not form damage, it is still greatly reduced in comparison with the dry case.

In an experimental study, the sliding and impact speeds and the lubricant viscosity were varied to ascertain their effect on wear (Ref 4). The results are illustrated in Fig. 15. As can be seen, the highly viscous lubricant prevented all wear involving a sliding component. The less viscous lubricant allowed wear at high impact velocities but prevented wear at low impact velocities. Results for the lighter lubricant indicate that normal impact is more damaging than compound impact.

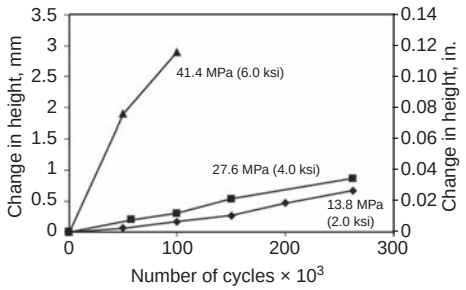

Fig. 10 Height change versus number of compound-impact cycles for aluminum 2011-T3 specimens tested against 17-4 PH stainless steel counterfaces with varying impact stresses (sliding velocity 5.33 m/s, or 17.5 ft/s). Source: Ref 8

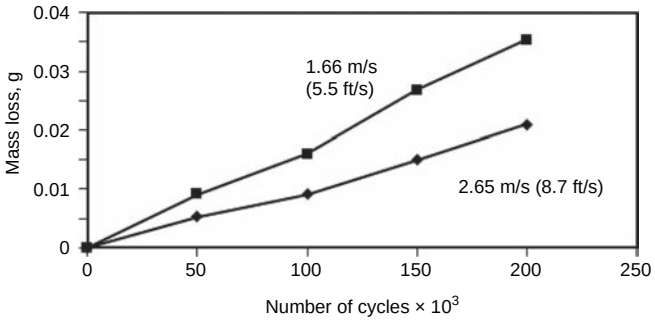

Fig. 11 Mass loss versus number of compound-impact cycles for aluminum 2011-T3 specimens tested against 17-4 PH stainless steel counterfaces with varying sliding velocities (impact stress: 10.8 MPa, or 1.6 ksi). Source: Ref 8

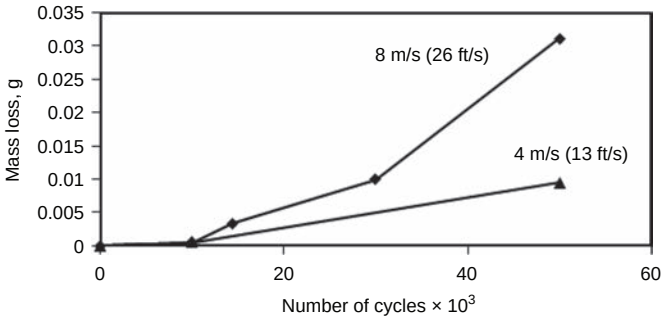

Fig. 12 Mass loss versus number of compound-impact cycles for 17-4 PH stainless steel counterfaces tested with CPM-10V steel specimens (impact stress: 69 MPa, or 10 ksi). Source: Ref 31

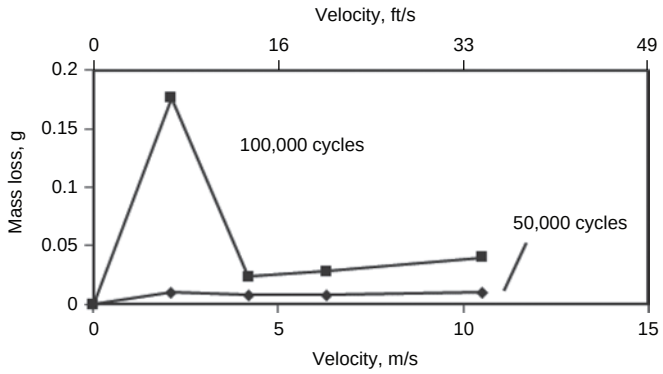

Fig. 13 Mass loss versus sliding velocity for compound-impact testing of titanium alloy RMI 5522S specimens against 17-4 PH stainless steel counterfaces (impact stress: 18.6 MPa, or ksi). Source: Ref 23

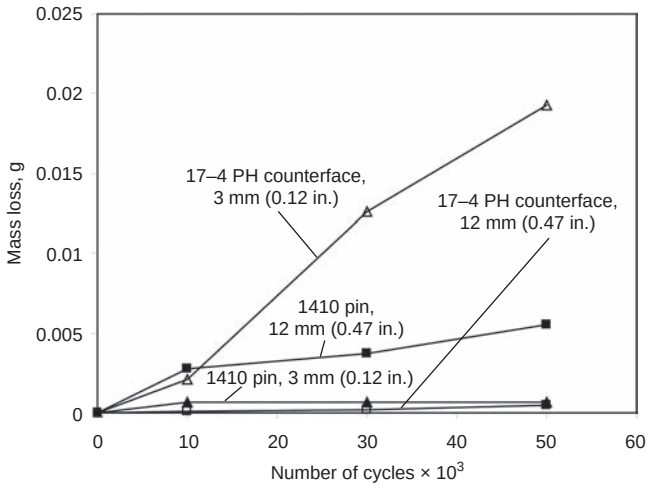

Fig. 14 Mass loss versus number of compound-impact cycles for 1410 steel specimens of varying length run against 17-4 PH stainless steel counterfaces (impact stress: 69 MPa, or 10 ksi; sliding velocity: 10 m/s, or 33ft/s). Source: Ref 24

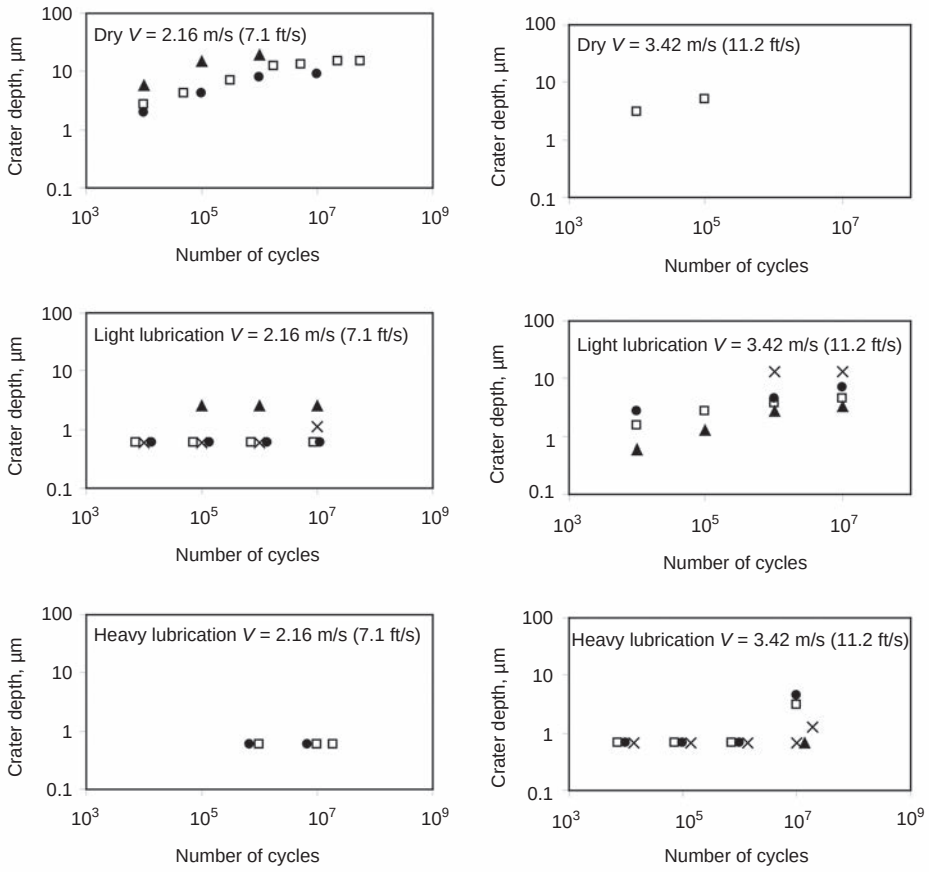

Fig. 15 Results of lubricated compound-impact wear experiments. V = impact velocity and v = sliding velocity; x: v = 0 m/s (0 ft/s); ●: = 0.25 m/s (0.8 ft/s); □: v = 1.27 m/s (4.2 ft/s); ▲: v = 3.81 m/s (12.5 ft/s). Source: Ref 4

Fricke and Allen (Ref 29) carried out tests with water lubrication, showing that wear rates half those in an equivalent dry contact could be achieved.

Impact Angle

The effect of impact angle on wear has been characterized for metals (Ref 38, 39). The general trend is that the lower the impact angle, the higher the wear (where the impact angle is defined as that between the counterface and the path of the impacting specimen). Maximum wear was found at approximately 30°, where the shear and induced sliding are at their highest. As the impact angle increases toward a normal impact, the wear mechanism changes as shear decreases, and there is less sliding. At this point, damage is more typically indentation-associated plastic flow and perhaps crack formation in more brittle materials. The same behavior has been exhibited by ceramics at low angles, but the wear minima occur at approximately 60°. Normal impact has a far greater effect on brittle ceramics than on more ductile metals (Ref 40), because wear rises considerably from 60 to 90°.

Temperature

In compound-impact tests, it was found that wear rose as the temperature was increased to 200 °C (390 °F) from room temperature, as the steel being tested softened (Ref 41). However, a further increase to 400 °C (750 °F) decreased wear rates to well below those at room temperature.

Low-temperature compound-impact tests down to −60 °C (−75 °F) have also been carried out on martensitic steels (Ref 42). Wear was largely independent of temperature over the range tested. However, the impact craters of the samples tested at lower temperatures showed more microcracks stemming from the opening of grain boundaries.

Wear Debris

The size and shape of wear debris particles arising from normal and compound wear vary depending on the material pair and the nominal levels of stress and sliding velocity in the contact. Analysis of wear debris from a range of experiments carried out mainly with titanium alloy specimens impacting 17-4 PH stainless steel counterfaces at varying contact conditions (impact stress: 6.9 to 69 MPa, or 1 to 10 ksi; sliding velocity: 0.01 to 10 m/s, or 0.03 to 33 ft/s) has shown that (Ref 43):

- Most observable wear particles fell in the range 0.3 to 0.7 mm (0.01 to 0.03 in.).
- In general, the shape was platelike.
- A preferred crystallographic orientation exists, as would be expected from the sliding direction.

Observations were also made that indicate:

- Debris stems from both specimen and counterface materials.
- Metallic particles consist of small and/or distorted primary crystals.
- Oxide formation occurs.
- Phase transformation of the metallic constituents may occur.

The occurrence of oxides in the wear debris indicates that oxygen plays a part in the wear

process itself. It is probable that at least a portion of the oxides found in debris are formed while the particles are still attached to the substrate at the contact interface, although oxidation will also occur after the particles have been broken away from the wear surface.

Phase transformations can provide evidence of local temperatures and/or stress fields and/or interdiffusion of species from surrounding materials (Ref 43). In the tests outlined earlier, it was found, for example, that the 17-4 PH stainless steel yielded debris containing γ-iron (austenite). To transform the martensitic state of the 17-4 PH stainless steel, a temperature of at least 500 °C (930 °F) is required.

Impact Wear of Ceramics

Material-Removal Mechanisms

In both normal impact and compound impact with tangential contact involving ceramic bodies, mechanical energy is expended partly in frictional heating and in mechanical deformation that leads to wear (Ref 40). Brittle and plastic modes of material removal occur during impact. Brittle deformation is linked to the creation of pits (formed when material is adhesively plucked from the surface of one impacting body by the other), partial ring cracks, and delamination layers. The removed material is pulverized and compacted. At acute contact angles, where the largest slip occurs, the wear debris is also sheared, transferred, and redeposited.

Delamination is generally the dominant wear process. It causes extensive material removal and occurs at all contact angles. Figure 16 illustrates four stages of delamination (Ref 40). Stage 1 involves the fracturing of substrate material and crushing of wear debris. The depth of fracturing, which is less than the average grain dimension, is governed by the normal pressure applied. Eventually, the layer of debris becomes thick enough to cushion and redistribute the normal stress in the substrate. The impact energy then acts to extrude the debris into interstices, and a thin, fine-grained film is created (stage 2). The interface between the film and the substrate is a zone of weakness in which cracks can nucleate (stage 3). Lateral propagation and intersection of the cracks results in the delamination of platelike debris (stage 4).

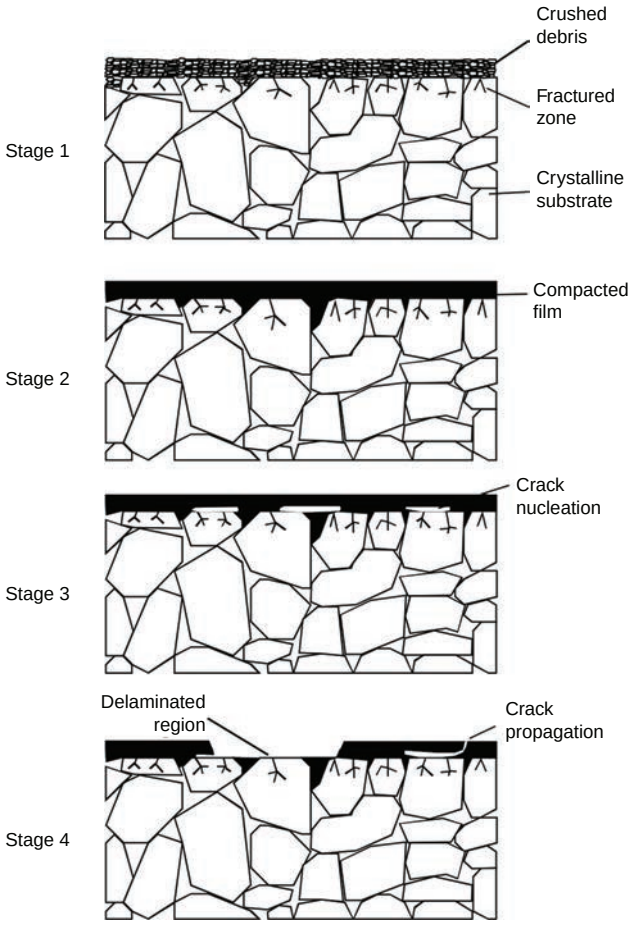

Fig. 16 Schematic diagram of the stages of delamination caused by repeated impact on a ceramic surface. Stage 1, fracturing on the surface and crushing of debris; stage 2, extrusion of pulverized debris in interstices and compaction of a fine-grained film; stage 3, nucleation of cracks along the weak film/substrate interface; and stage 4, lateral propagation of interfacial cracks and delamination of the compacted film. Source: Ref 43

Influences on Wear

In repetitive impact of ceramics, two factors influence the magnitude of wear experienced. The first factor is associated with the normal stress that is partly accommodated in the brittle fracture of the parent materials. The effect of normal stress on wear increases as the angle of contact increases. The second factor is related to the tangential stress and accelerates delamination of the protective surface film. The influence of shear decreases as the angle (from 45 to 90°) of contact increases. A model illustrating the dependency of impact wear to angle of contact is shown in Fig. 17 (Ref 40). The model shows that the combined effect of the normal and tangential stresses is minimized between these angles.

Relative humidity has a pronounced effect on the wear mechanism and material-removal rate during the repetitive impact of ceramics (Fig. 18). In dry conditions, as described earlier, extensive fracture and growth of cracks is promoted along grain boundaries. In humid conditions, fracture only happens on a small scale due to the occurrence of crack-arrest mechanisms, and consequently, wear rates are reduced.

The machined surface finish has an influence on wear during early cycles of impact, as shown in Fig. 19 (Ref 45). Wear rates of ground bodies are higher than polished bodies because the latter is protected by a film of oxidized wear debris. The wear behavior of a ground surface is characterized by the lateral extrusion of elongated ridges and then microfracture of extruded slivers. At higher numbers of impacts, the wear rates of polished and ground specimens are almost the same and are characterized by the mechanism outlined in Fig. 16.

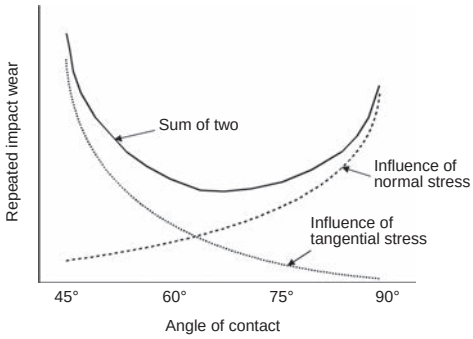

Fig. 17 Schematic illustration of the dependency of the repeated impact of a ceramic object on the angle of contact. Source: Ref 40

Machining residual stresses also affect wear. The results shown in Fig. 20 (Ref 46) indicate that impact wear decreases with increasing compressive residual stress. It has been suggested that this reduction in wear at high residual stresses results from crack growth being impeded (Ref 45).

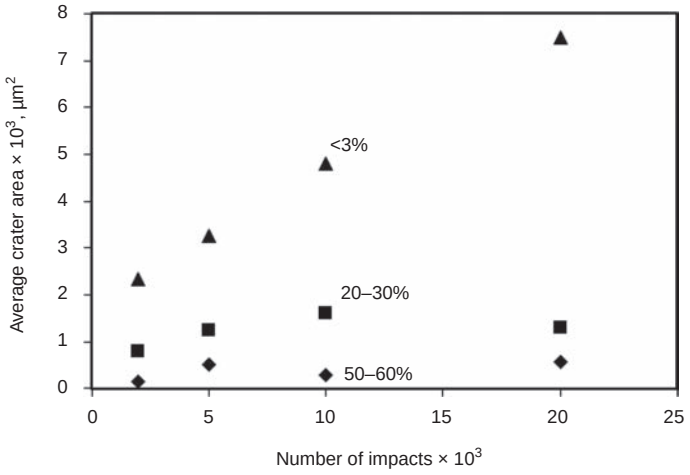

Fig. 18 Average crater area versus number of impacts for SN220M silicon nitride counterfaces impacted with a SN220M silicon nitride ball at varying humidities. Source: Ref 44

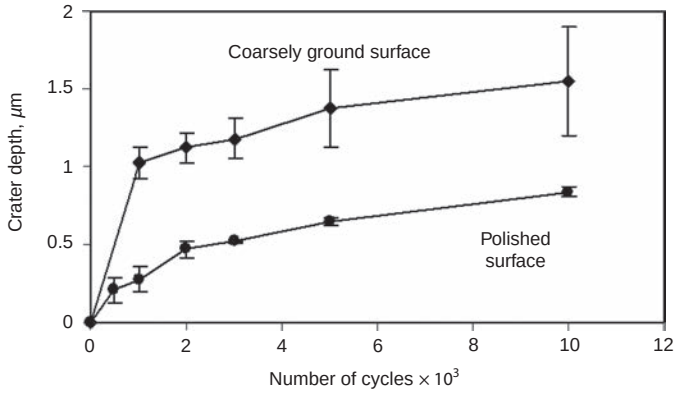

Fig. 19 Crater depth versus number of impacts for GS-44 silicon nitride counterfaces of varying surface finish impacted with a NBD-200 silicon nitride ball. Source: Ref 45

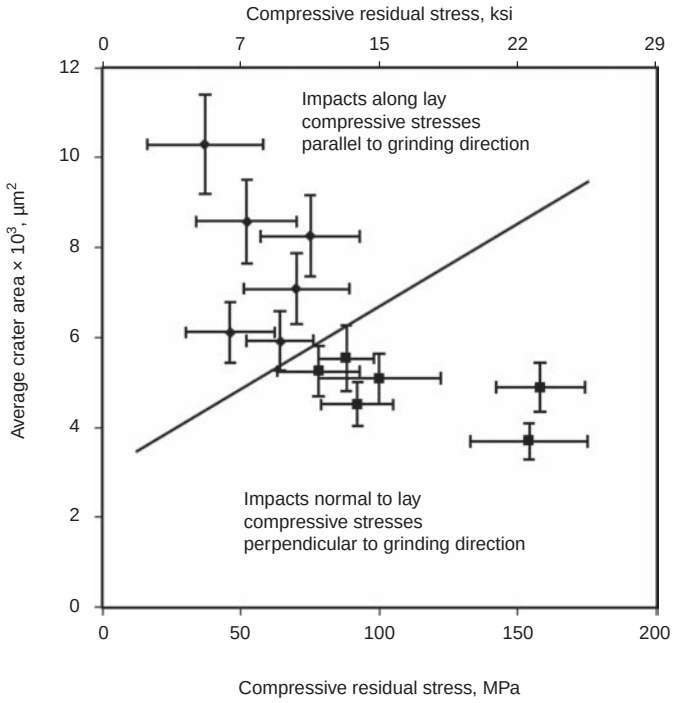

Fig. 20 Impact crater area versus compressive residual stress for impacts normal to the lay and compressive stresses perpendicular to the grinding direction (■) and for impacts perpendicular to the lay and compressive stresses parallel to the grinding direction (●), using sintered reaction-bonded silicon nitride counterfaces and NBD-200 silicon nitride balls. Source: Ref 46

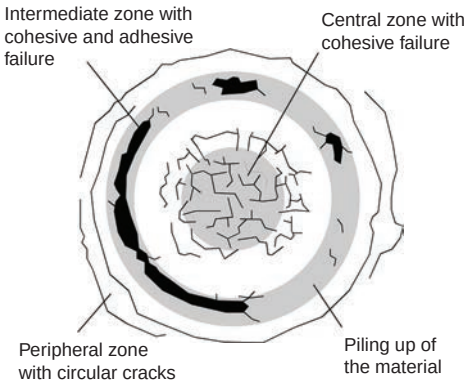

Fig. 21 Schematic diagram of a typical indentation formed in a ceramic coating under repetitive impact loading showing different failure zones. Source: Ref 47

It can also be seen that grinding results in compressive residual stresses that are typically larger in magnitude in the direction perpendicular to the grinding direction than in the direction of grinding.

Impact Failure of Ceramic Coatings

Hard coatings are becoming widely used to increase wear resistance of machine parts subjected to repetitive normal impacts or tools used in cutting or cold forming. The thin layers of coating can be deposited on any steel component using sputtering techniques, allowing economy in the use of expensive materials. Three different failure zones are apparent in ceramic coatings, such as TiN and TiC (Ref 47), as shown in Fig. 21, which illustrates a typical indentation formed in a ceramic coating subjected to repetitive impacting by a hardened steel ball. A central zone of cohesive failure exists in which cracking and coating delamination occurs. An intermediate zone is found between the central and peripheral regions on the internal side of the rim formed around the indentation. The intermediate zone exhibits adhesive-cohesive failure of the coating under the buildup of shear stresses that arise from plastic strain of the substrate during impact. In hard brittle coatings, the high tensile stress in the immediate vicinity of the impact causes the development of a large number of cracks in the peripheral region of the impact.

A good correlation exists between increasing failure and the number of impacts. Increasing the number of impacts not only increases the number of cracks but also increases the wear at each crack before the coating eventually starts to delaminate or spall. Cracks arise when a hard coating is not tough or ductile enough to accommodate the stress of deformation under an impact.

Impact Wear of Polymers

Two modes of impact wear or damage of polymers have been observed (Ref 48). The first mode relates primarily to the plastic flow or deformation of the material without material loss. A second mode appears as the wear rate increases, and this is associated with material loss. In the material-loss mode, cracks appear in the surface.

For synthetic fluorine-containing resin and polyoxymethylene tested against 17-4 PH stainless steel counterfaces, wear rates for normal impacts at low stress were very low (Ref 49). In compound-impact wear, rates were higher and increased with sliding speed. Wear occurred by a mechanism of delamination. Wear debris in the form of platelets is particularly apparent in cases of compound impact. Increasing sliding speed tends to accelerate the process of surface and subsurface crack initiation, and increasing numbers of impact cycles tend to refine the microcrack patterns.

Polyoxymethylene is a relatively crystalline polymer; therefore, the conventional delamination theory based on the accumulation of dislocations leading to the nucleation of subsurface cracks may apply (Ref 27). Synthetic fluorine-containing resin, however, is relatively amorphous; therefore, an alternative to the theory of delamination outlined previously is required. Part of the answer may be related to microvoids observed in polyimide films (Ref 50) as well as water clusters found to be introduced during the processing of polymers (Ref 51). Both, if present, could act as sites for the initiation of microcracks.

For impacts at higher stresses, several critical phenomena have been identified, such as charring and chemical degradation and the existence of a stress threshold beyond which catastrophic wear occurs (Ref 52).

Impact Wear Testing

Two different types of test rigs have been developed for impact wear studies: ballistic impact testers and reciprocating hammer testers (Ref 13). The following describes the features of each.

Ballistic Impact Wear Apparatus

In ballistic impact wear testers, repetitive impacts are achieved by firing projectiles at a counterface. To ensure the projectiles impact at the same point each time, guides are provided. Some test rigs use one projectile repeatedly impacting against a counterface (Ref 2, 17, 30), while others use a number of projectiles (usually balls) that are recycled (Fig. 22). Those using one projectile can be used for one-body wear investigations on the projectile with a hard, negligibly wearing counterface. By proper synchronization of projectile firing with rotational speed of the counterface to ensure impacts occur at the same point, two-body wear can also be studied. In those test rigs using a number of projectiles, clearly only the wear of the counterface can be investigated. Ballistic test rigs have two main disadvantages. The first is that, because of cleaning problems with the projectile guides, lubricated tests are difficult to carry out. The second is that it is sometimes difficult to retune the rigs to take different weight projectiles.

Reciprocating Hammer Impact Wear Apparatus

In reciprocating hammer impact wear test rigs, a hammer is made to impact a counterface. This can be by moving the hammer up and down via electrical or mechanical means. A stationary counterface is used for normal-impact studies, while for compound studies, shear is imparted by using a rotating counterface or by altering the tilt of the counterface to change the angle of contact. Again, synchronization is required for rotating counterfaces to ensure that impact occurs at the same point during each cycle. A number of reciprocating hammer test rigs are in existence that use an impacter at the end of a lever arm moved up and down through a rotating cam (Ref 36, 52, 53, 54). A typical example is shown in Fig. 23. Various mechanisms are employed to move the hammer up and down, including electromagnets and cams. Pivotal hammer test rigs overcome the contact lubrication and retuning problems encountered with ballistic rigs. However, there are problems associated with the flexure arising in the hammers, and the elastic vibrational modes of the hammers may complicate analysis. Alignment problems are also more likely to arise with pivotal hammers than in ballistic rigs. This can mean that small tangential oscillations are induced between hammer and counterface, leading to surface damage by shear tractions.

Specific apparatus to allow abrasive media to be fed into an impacting hammer contact has now been developed (Ref 5, 6). An example is shown in Fig. 24.

Impact Wear Modeling

An impact wear modeling approach has been established based on two stages of wear progression (Ref 13). The first is an induction period (Fig. 25), during which deformation occurs and a wear scar is formed, but there is no measurable material loss. The end of this stage is defined as the zero wear limit. This constitutes the initial point of the measurable wear region. As indicated in Fig. 25, the progression of wear in this region can take on a number of forms. These will depend on the mechanism of wear, which is

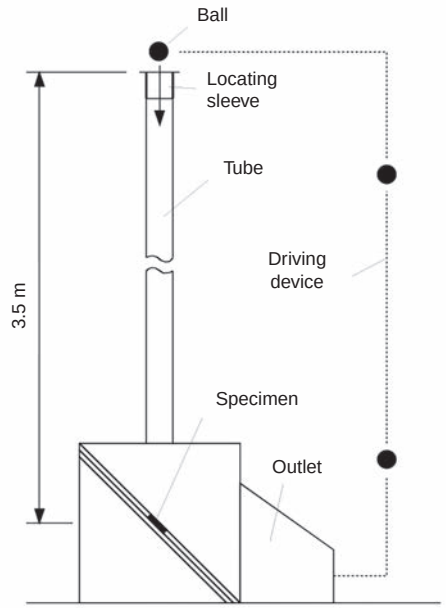

Fig. 22 Ballistic impact wear tester. Source: Ref 25

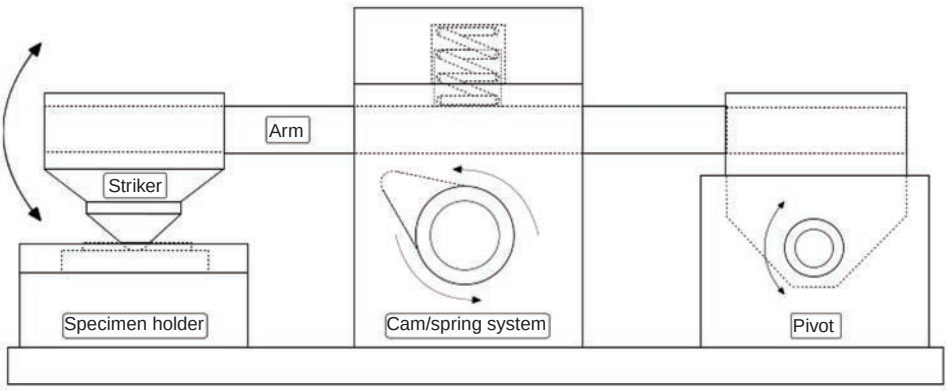

Fig. 23 Reciprocating hammer impact tester. Reprinted from Ref 36 with permission from Elsevier

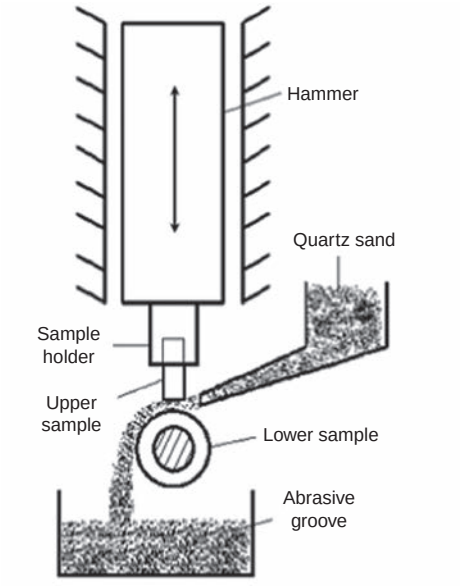

Fig. 24 Abrasive impact wear testing equipment. Reprinted from Ref 6 with permission from Elsevier

related to the impacting material and the severity of the contact conditions.

Most mechanical components continue to be functional beyond the zero wear limit, and their usefulness is normally connected with the loss of a specific depth of material. For that reason, the measurable wear process is probably of more interest to an analyst attempting to define a life prediction for a repetitively impacted component.

Zero Impact Wear Model

The following equation has been developed to establish a quantitative, semiempirical evaluation of the zero wear limit for specimens subjected to repetitive compound impacts in the elastic stress region (Ref 13). It considers wear damage to be contributed from the surface shear stress, τ_2, and the maximum subsurface shear stress, τ_1, during each impact:

$$N_0 = \frac{1}{1+\beta}\left(\frac{\gamma\sigma_y}{\sigma}\right)^9 2000 \qquad \text{(Eq 1)}$$

where N_0 is the number of cycles at which the zero limit is reached, σ_y is the uniaxial tensile yield stress, σ is the peak Hertzian pressure, and γ is a material wear factor (experiments have shown that γ is approximately 1.1 for carbon and tool steel specimens) (Ref 55). The quantity β is the ratio of the surface damage contribution, D_1, to the subsurface damage contribution, D_2, where:

$$D_1 = \int_0^{t^*} \tau_1^9(t)dt \qquad \text{(Eq 2)}$$

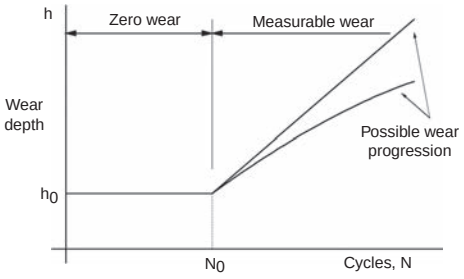

Fig. 25 Zero and measurable wear. Source: Ref 13

$$D_2 = \int_{0\bar{t}} \tau_2^9(t)dt \qquad \text{(Eq 3)}$$

$$\beta = \frac{D_1}{D_2} \qquad \text{(Eq 4)}$$

where t^* is the duration of the impact force pulse. The integral in Eq 3 is evaluated between $t = 0$ and $t = \bar{t}$, where $\bar{t}$ is the slipping time. This signifies that in compound impact with sliding, wear is only occurring in the initial phase of contact, while slipping is taking place between the specimen and the counterface.

Measurable Impact Wear Models

Approaches for modeling measurable impact wear include a linear model based on an Archard-type wear law (Ref 3). Starting with the relationship for wear volume, W:

$$W = \frac{kPx}{H} \qquad \text{(Eq 5)}$$

where P is the load (in Newtons), x is the sliding distance (in meters), H is the hardness, and k is a nondimensional wear coefficient. Load can be replaced by friction force divided by the friction coefficient, μ. Friction force multiplied by the sliding distance represents the energy dissipated in sliding. If α is defined as the proportion of the total impact energy expended in interfacial slip, and the term $(\alpha k/\mu)$ is replaced by a parameter K, then if I is the energy of impact and n the number of impacts, wear volume can be defined as:

$$W = \frac{KIn}{H} \qquad \text{(Eq 6)}$$

where K is now the nondimensional impact wear coefficient.

As stated previously, K is related to k by the following expression:

$$K = \frac{k\alpha}{\mu} \qquad \text{(Eq 7)}$$

The nonelastic part of an impact has been estimated as being 70% (based on rebound measurements of a striking hammer) (Ref 3), and only a small amount of this would be expended in shear at the interface, so α would be small, for example, 10%. The friction coefficient, μ, for an unlubricated contact generally falls in the range of 0.5 to 1, so it would be expected that K would be approximately an order of magnitude smaller than the sliding wear coefficient, k. For unlubricated metals, k is generally in the range of 5×10^{-3} to 3×10^{-5}, while K values between 5×10^{-4} and 1×10^{-6} would be anticipated. The majority of the values for K given in Table 1, determined from a range of experiments carried out with different material and contact conditions, fall within this range.

A relationship of the same form as that used in erosion studies to model wear mass, W (Ref 56), which gives a declining wear rate, has also been used successfully to predict wear in percussive impact of large bodies (Ref 29, 58):

$$W = KNe^n \qquad \text{(Eq 8)}$$

where e is the impact energy per cycle (in Joules), N is the number of cycles, and K and n are empirically determined wear constants, and:

$$e = \frac{1}{2}mv^2 \qquad \text{(Eq 9)}$$

where m is mass (in kilograms), and v is the valve velocity at impact (in meters per second).

A variation of the Wellinger and Breckel model (Ref 56) has emerged recently from Akhondizadeh et al. (Ref 59):

$$W = KV^{\alpha}r^{\beta}e^{\theta\gamma} \qquad \text{(Eq 10)}$$

where W is the wear loss, V is the impact velocity, r is the ball radius, e is the impact energy, θ is the impact angle, and α, β, γ, and K are constants. The model was formed using a Taguchi method for design of experiments with level 4 and 16 tests. Taguchi is good for linear relationships, while the results of impact tests obtained in the experiments are nonlinear, which makes Taguchi unsuitable for effectively predicting the interactions between parameters.

Impact Wear Case Studies

Two case studies are presented that represent two different levels of testing. The first uses a hammer impact rig to study material performance; the second uses actual components to simulate an accurate contact geometry.

Material Performance and Simulation Testing to Examine Impact Wear

Fundamental Case Study: Use of Induction Hardening to Improve Impact Wear Resistance of Cast Iron.

The continuing development and improvement of machines and engineering components

means that previously unseen or insignificant problems can manifest themselves in "known good" designs and material choices. Even in situations where components themselves have not changed significantly, the operating conditions may have been altered, which can promote wear.

The increased use of a type of cast iron known as compacted graphite iron (CGI) often results from this conundrum, because it can offer increased strength, when compared to aluminum alloys, and reduced weight, when compared to other cast irons. Although denser than aluminum, the greater strength of CGI compared to typical aluminum alloys means that much thinner wall thicknesses can be used. For example, the overall mass of a complete component is comparable to that of a predominantly aluminum alloy equivalent.

That said, the impact wear resistance of as-cast CGI is comparable to the more traditional cast irons in a similar state, so surface treatment is still required to minimize wear. Therefore, it is sensible to evaluate the use of a common surface treatment (e.g., induction hardening) to improve the wear resistance (e.g., impact wear) of the material, regardless of its use in an engineered component.

Using a typical reciprocating hammer impact wear apparatus, Slatter et al. (Ref 36) generated impact wear scars on small disc-shaped specimens 50 mm (2 in.) in diameter and 10 mm (0.4 in.) thick, all made from CGI of the same composition. The surface of each specimen was ground to maintain constant surface topography, with a roughness average (R_a) of approximately 0.5 μm. Chrome steel balls, 15 mm (0.6 in.) in diameter, were used as strikers, and they impinged, in free flight, into the center of the specimen at 10 Hz. The arrangement of the specimen holder and striker arm/holder was such that the balls strike normal to the specimen surface to avoid any sliding wear.

Three sets of specimens were produced. One set was left untreated to investigate the fundamental impact wear resistance of CGI and to act as a control. Another two sets of specimens were subjected to two levels of induction hardening, one set to a nominal case-hardened depth of 2 mm (0.08 in.) and another set to a nominal case-hardened depth of 3 mm (0.12 in.).

A custom inductor was manufactured to suit the geometry of the specimens, and all specimens were treated equally. The only difference was the nominal, or target, hardening depths of 2 and 3 mm. Before any testing was performed, hardness measurements were taken of the specimens, using a load of 10 N (2.2 lbf) for a duration of 10 s. For the induction-hardened specimens, a single sample was taken from each of the two specimen sets and was sectioned. A single hardness measurement was taken at 0.5 mm (0.02 in.) intervals across the depth of the section. The hardness measurements at various depths through each of the two sample specimens are plotted in Fig. 26. As can be seen, induction hardening raised the hardness at the specimen surfaces to 650 to 700 HV. The hardness of the untreated specimens was assumed to be uniform at 250 HV throughout.

After testing, the wear scars were examined, and, when visible, the wear debris from the untreated specimens consisted of much finer dark particles when compared to the treated specimens. In the case of the specimen shown in Fig. 27 of an untreated specimen that was subjected to 72,000 impacts, there is a considerable amount of wear debris. The dark, egg-shell-like markings and lines visible on the surface of the scar in Fig. 27(b) are a result of pickup, transfer, and deformation of wear debris by the striker, as well as the wear not being severe enough to remove machining (grinding) marks.

Figure 28 shows the wear scar present on the specimens, hardened to a nominal depth of 2 mm (0.08 in.), after 72,000 impacts. There was little visible wear debris compared to the apparent size of the wear scar, indicating that there was also likely to be displaced material. In Fig. 28(b) and (c), machining marks from the manufacture of the specimen are still visible around the edge of the wear scar, indicating that not much wear has occurred and the initial slope of the wear scar crater is shallow.

On the surface of the specimens that were hardened to a nominal depth of 3 mm (0.12 in.), again after 72,000 impacts, a large

Table 1 Impact wear coefficient values

Reference	Surface measured	Impact energy, kgf · mm	No. of impacts	Lubrication	Impact wear coefficient, K
Ref 16	Copper (hard)	2	1	N	53×10^{-6}
	Steel	20	1	N	67×10^{-6}
	Steel	20	1	Y	10×10^{-6}
Ref 15	Tungsten	138	2.4×10^{3}	N	130×10^{-6}
Ref 56	Copper	60	5×10^{5}	N	20×10^{-6}
	Soft steel	120	5×10^{5}	N	19×10^{-6}
	Aluminum alloy	60	5×10^{5}	N	42×10^{-6}
	Titanium alloy	120	5×10^{5}	N	15×10^{-6}
	Hard steel	160	5×10^{5}	N	28×10^{-6}
	Hard steel	700	4×10^{3}	N	43×10^{-6}
	Hard steel	42	2×10^{4}	N	104×10^{-6}
Ref 4	Hard steel	0.36	6.5×10^{4}	N	14×10^{-6}
	Hard steel	0.36	4.3×10^{5}	Y	1.2×10^{-6}
	Soft steel	0.36	1×10^{4}	N	247×10^{-6}
	Soft steel	0.36	3.2×10^{6}	Y	0.8×10^{-6}
Ref 13	Hard steel	0.48	10^{7}	N	0.2×10^{-6}
Ref 57	Soft steel	110	800	N	930×10^{-6}
	Nickel	110	1300	N	850×10^{-6}
	Titanium alloy	110	500	N	99×10^{-6}
	Aluminum bronze	110	500	N	370×10^{-6}
	Chrome plate	110	2000	N	1200×10^{-6}
	Soft steel	110	500	Y	24×10^{-6}

Source: Ref 57

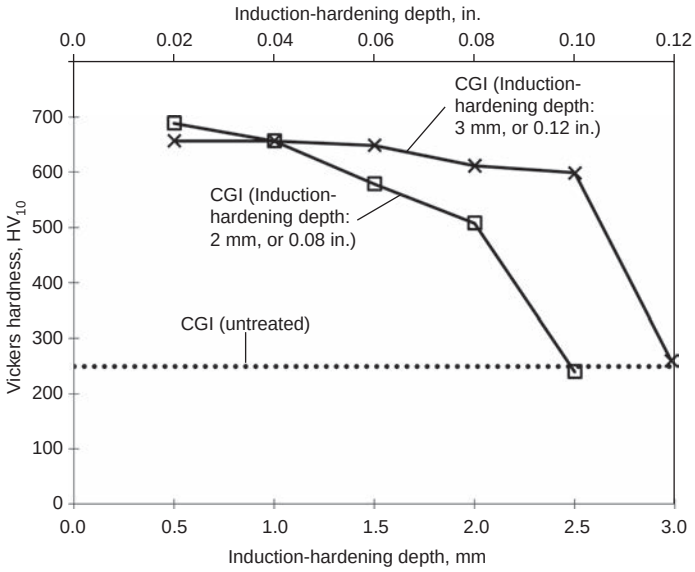

Fig. 26 Hardness profile of treated and untreated compacted graphite iron (CGI). Source: Ref 36

number of shiny, metallic, rough-edged particles were visible and were significantly larger than those found on the surface of the untreated specimens. Figure 29(a) is a general view of the specimen surface, and false color has been used to highlight the extent of the wear debris. There are no machining marks visible (Fig. 29(b), indicating that more wear occurred in these specimens. The lack of machining marks could also indicate that the material has been removed rather than merely displaced, indicating a lack of plastic deformation. Similarly, the wear scar crater edge again appears to be quite rough, so it likely fractured before flowing.

After testing, the wear scars were measured using a profilometer. The results (Fig. 30–32) clearly show the improved wear resistance of the treated CGI but also the importance of optimizing the nature (in this case, nominal hardening depth) of the surface treatment. It is important to note that for similar magnitudes of "damage" relative to the untreated specimens, the shallower treatment allows material to be displaced away from the contact, whereas the deeper treatment promotes material being removed from the surface entirely. These data also illustrate that the nature of the wear mechanisms involved can be very sensitive to small changes in what may be considered a relatively uniform section of material. In this case, the exact slope of the hardness profile through the surface generated by the hardening process and the exact position of the peak subsurface stress have caused quite different wear mechanisms for measurable wear an order of magnitude or smaller than the nominal case-hardening depth.

Whether or not these two situations are considered the same is dependent on the machine element contact the material is eventually used in. This can be an important aspect to consider, for example, in situations where some wear in a contact is acceptable, but wear debris leaving the contact and contaminating the rest of the system or the product it produces is unacceptable.

Component Failure Case Study: Automotive Engine Inlet Valve and Seat Wear.

The drive for reduced oil consumption and exhaust emissions has led to a reduction in

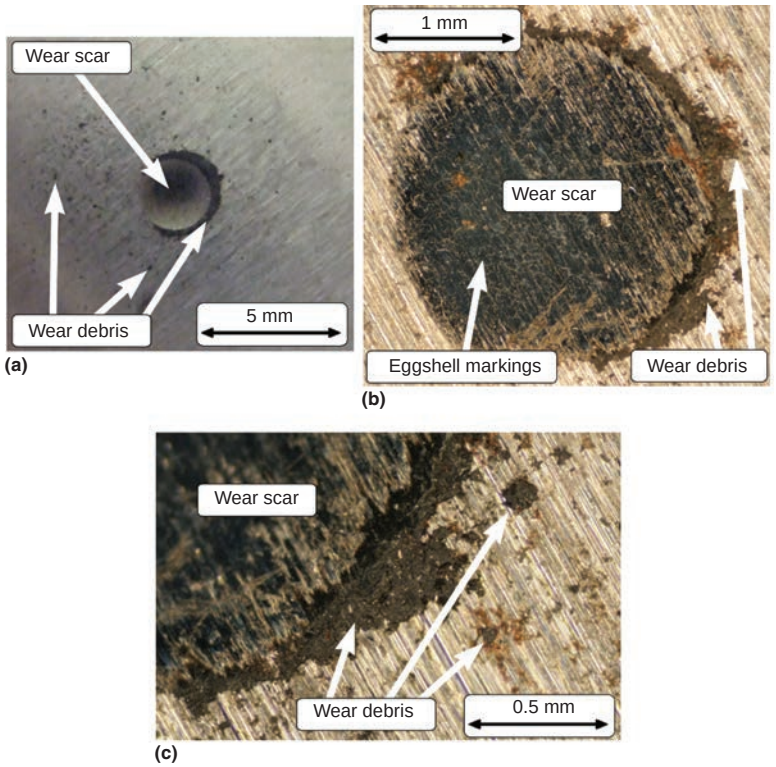

Fig. 27 Wear scar and wear debris from an untreated compacted graphite iron specimen after 72,000 impacts. Reprinted from Ref 36 with permission from Elsevier

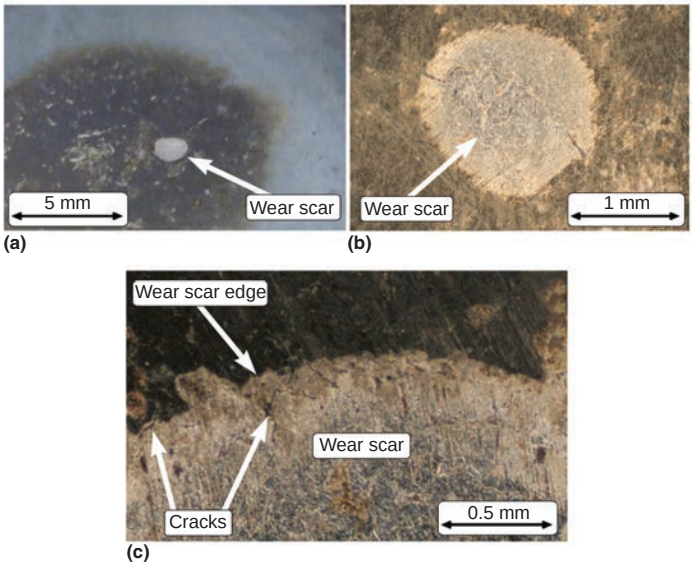

Fig. 28 Wear scar and wear debris from a 2 mm (0.08 in.) induction-hardened compacted graphite iron specimen after 72,000 impacts. Reprinted from Ref 36 with permission from Elsevier

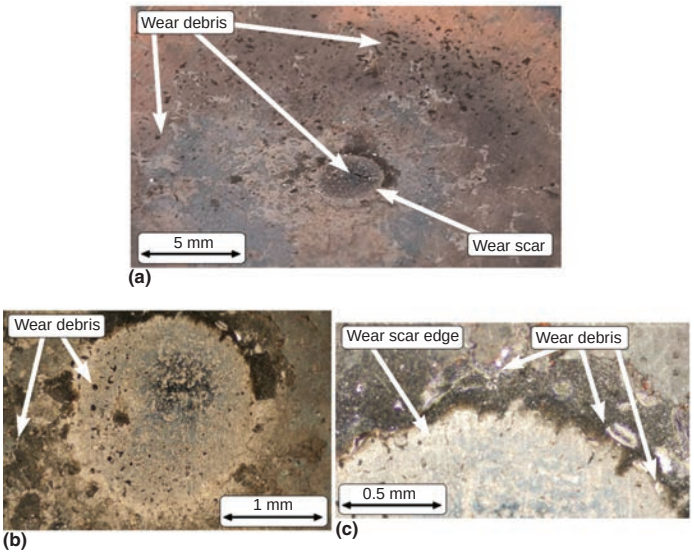

Fig. 29 Wear scar and wear debris from a 3 mm (0.12 in.) induction-hardened compacted graphite iron specimen after 72,000 impacts. Reprinted from Ref 36 with permission from Elsevier

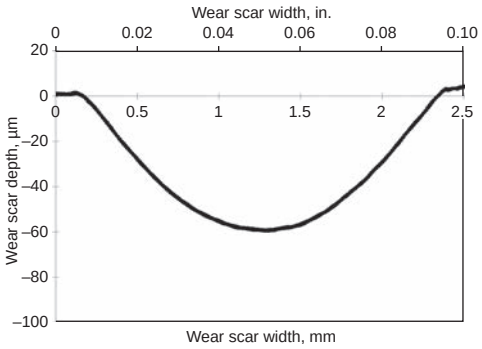

Fig. 30 Profile of wear scar on an untreated compacted graphite iron specimen after 72,000 impacts. Source: Ref 36

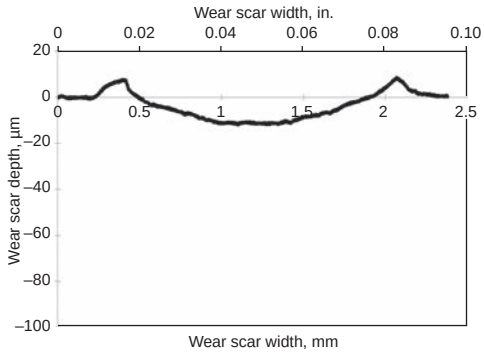

Fig. 31 Profile of wear scar on a compacted graphite iron specimen induction hardened to a depth of 2 mm (0.08 in.) after 72,000 impacts. Source: Ref 36

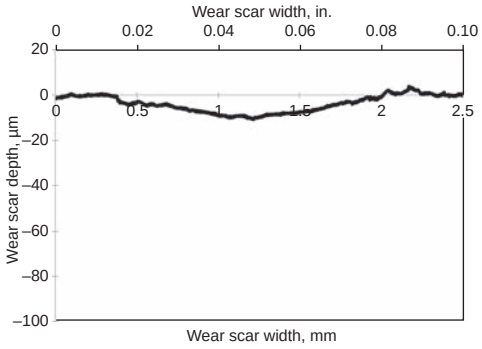

Fig. 32 Profile of wear scar on a compacted graphite iron specimen induction hardened to a depth of 3 mm (0.12 in.) after 72,000 impacts. Source: Ref 36

the amount of lubricant present in the air stream in automotive engines. This, combined with the effort to lengthen service intervals and increase engine performance, has led to an increase in the wear of inlet valves and seat inserts.

Engines are typically designed to tolerate a certain amount of valve recession (schematically represented in Fig. 33). After this has been exceeded, the gap between the valve tip and the follower must be adjusted to ensure that the valve continues to seat correctly. If the valve is not able to seat, cylinder pressure will be lost, and the hot combustion gases that leak will cause valve guttering or torching to occur that will rapidly lead to valve failure.

Work carried out to isolate the fundamental mechanisms of automotive engine inlet valve and seat wear used an experimental apparatus designed to simulate the loading environment and contact conditions to which a valve and seat insert are subjected (Ref 60–62). The results showed that recession originates from two processes: impact of the valve on the seat on valve closure, and sliding of the valve against the seat as the valve head deflects and wedges into the seat as combustion occurs in the cylinder. These processes produce characteristic wear features on valves and seats. Impact on valve closure leads to the formation of a series of ridges and valleys on valve seating faces (Fig. 34) and surface cracking on seat seating faces (Fig. 35). While both mechanisms are significant, impact on valve closure is the main contributor to valve recession (Ref 62).

Impact wear resistance has been related to material properties, as shown in Fig. 36, which plots the results of bench tests isolating impact of the valve on the seat, where the tougher cast seat insert material has worn less than the sintered seat insert material (both materials are based on a tool steel matrix). This is further exemplified in Fig. 37, where results of bench tests run on a range of materials are shown. The tougher materials gave lower valve recession.

As shown in Fig. 38, recession due to impact wear is roughly proportional to valve closing

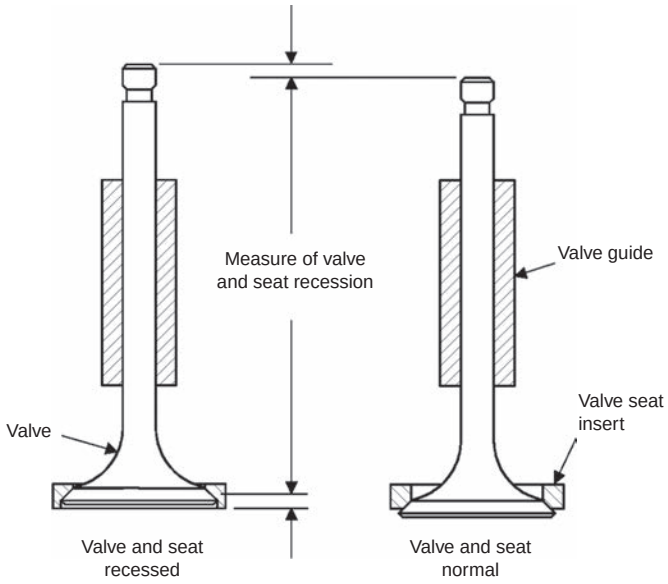

Fig. 33 Valve recession

velocity squared. This implies that wear is related to the energy of the valve on closing.

As a result, a relationship of the same form as that used in erosion studies to model wear mass, W (Ref 56) (based on impact energy) (Eq 8), was used to model wear due to the impact of the valve on the seat during valve closure (Ref 58). In this case, the impact energy (Eq 9) was determined using the mass of the valve and follower added to half the mass of the valve spring and the valve velocity at impact.

Values of K and n were derived using an iterative process to fit Eq 8 to experimental data. At each data point, the velocity was recalculated to take account of the change in lift due to recession. The results of this process for tests run with a cast seat insert (based on a tool steel matrix) are shown in Fig. 39. As can be seen, the model produces good correlation over a range of velocities.

The equation for impact wear was combined with an equation for sliding wear (based on an Archard-type wear law, Ref 63) to give an overall wear model (Eq 11). To incorporate

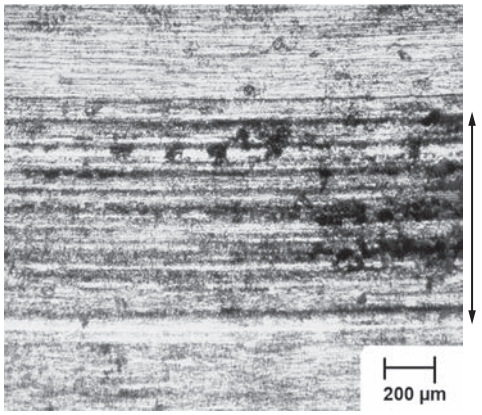

Fig. 34 Valve seating face showing a series of ridges and valleys formed circumferentially around the axis of the valve

the change in pressure at the interface and any other effects likely to lead to a reduction in the wear rate with time, such as work

hardening, a term consisting of the ratio of the initial valve/seat contact area, A_i, to the contact area after N cycles, A, to the power of a constant j was included. A value of 10 for j was determined empirically using bench and engine test data:

$$V = \left(\frac{k\overline{P}N\delta}{H} + KNe^{n}\right)\left(\frac{A_i}{A}\right)^{j} \quad \text{(Eq 11)}$$

where $\overline{P}$ is the average load at the valve/seat interface during combustion in the cylinder (in Newtons), k is a sliding wear coefficient, δ is the slip at the valve/seat interface, and H is the hardness of the softer material.

Equation 11 gives a wear volume, which is then converted to a recession value, r, using equations derived from the seat geometry. Equation 12 gives r in terms of V for the case where valve and seat angles are equal:

$$r = \left(\sqrt{\frac{V}{\pi R_i \cos\theta_s \sin\theta_s} + w_i^{2}} - w_i\right)\sin\theta_s \quad \text{(Eq 12)}$$

where R_i is the initial seat insert radius, θ_s is the seat insert seating face angle, and w_i is the initial seat insert seating face width (as measured). R_i can be calculated using w_i and the radius and seating face width as specified for the seat insert (R_d and w_d).

Results of model predictions for engine tests carried out using tool-steel-based cast and sintered seat inserts are shown in Fig. 40. As shown in Fig. 41, the contribution due to impact, as predicted by the model, is far greater than that of sliding.

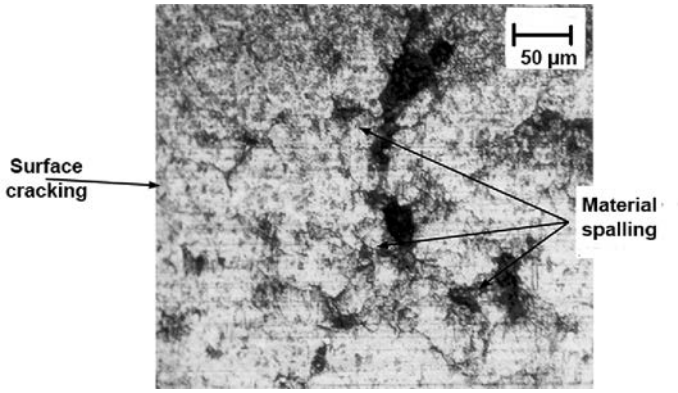

Fig. 35 Seat insert seating face showing surface cracking and subsequent material spalling

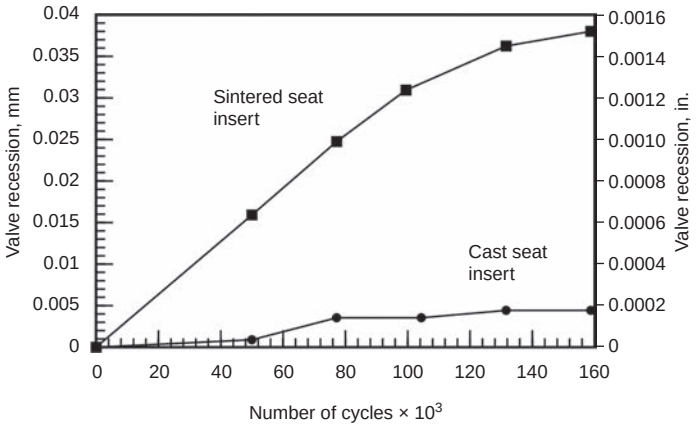

Fig. 36 Valve recession as a result of bench tests carried out isolating impact using a cast and a sintered seat insert material (both based on a tool steel matrix)

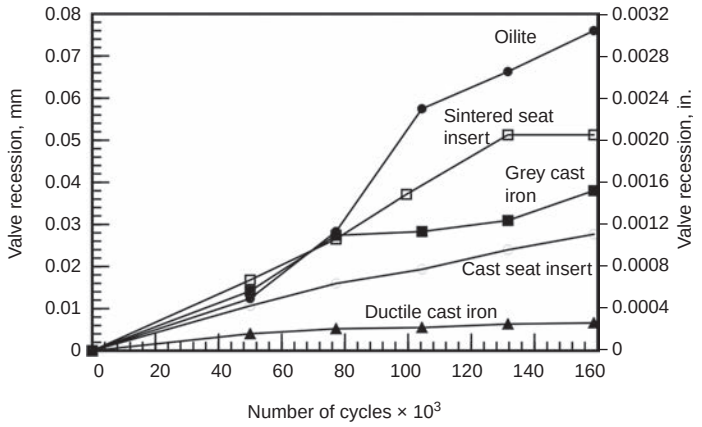

Fig. 37 Valve recession as a result of bench tests carried out isolating impact using a number of different seat materials

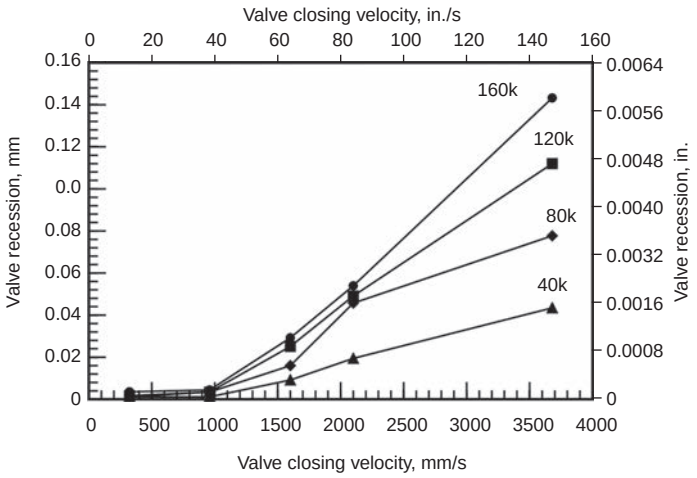

Fig. 38 Valve recession versus valve closing velocity for a series of bench tests carried out isolating impact using a cast tool steel based seat insert material

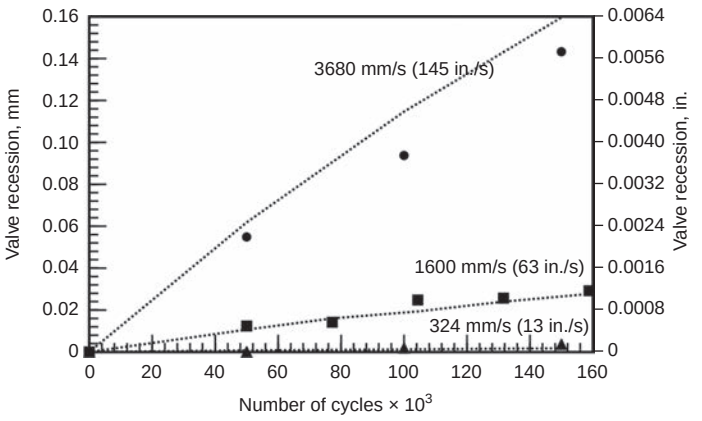

Fig. 39 Model predictions for valve recession caused by impact wear. Lines represent model predictions; data points represent bench test results.

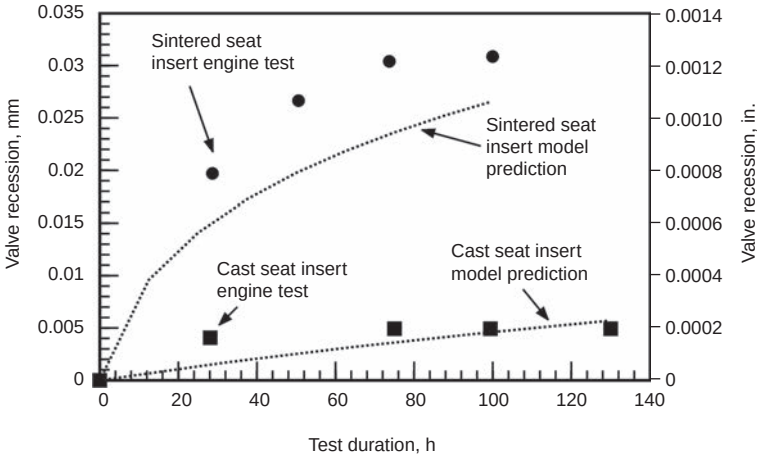

Fig. 40 Valve recession predictions using the combined impact-sliding model

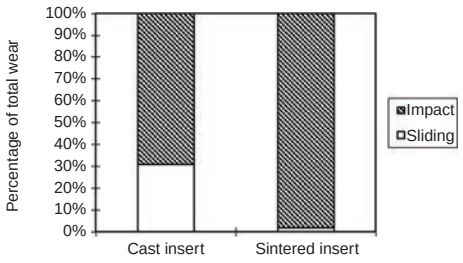

Fig. 41 Percentage of total valve recession caused by impact and sliding

ACKNOWLEDGMENT

This article was revised from R. Lewis and R. Dwyer-Joyce, "Impact Wear Failures," *Failure Analysis and Prevention*, Volume 11, *ASM Handbook*, ASM International, 2002, p 965–974.

REFERENCES

1. P.A. Engel, *Impact Wear, Friction, Lubrication, and Wear Technology,* Vol 18, *ASM Handbook,* ASM International, 1992, p 263–270
2. A.W.L. De Gee, C.P.L. Commissaris, and J.H. Zaat, The Wear of Sintered Aluminium Powder (SAP) Under Conditions of Vibrational Contact, *Wear,* Vol 7, 1964, p 535–550
3. E. Rabinowicz and K. Hozaki, *Impact Wear of Ductile Metals*, *Proc. JSLE International Tribology Conference* (Tokyo, Japan), 1985, p 263–268
4. P.A. Engel and J.L. Siroco, Impact Wear Study of Lubricated Contacts, *Trans. ASLE,* Vol 18, 1975, p 279–289
5. S.-G. Peng, R.-B. Song, T. Sun, F.-Q. Yang, P. Deng, and C.-J. Wu, Surface Failure Behavior of 70Mn Martensite Steel under Abrasive Impact Wear, *Wear,* Vol 362, 2016, p 129–134
6. S. Ge, Q. Wang, and J. Wang, The Impact Wear-Resistance Enhancement Mechanism of Medium Manganese Steel and Its Applications in Mining Machines, *Wear,* Vol 376, 2017, p 1097–1104
7. S.L. Rice, A Review of Wear Mechanisms and Related Topics, *Proc. Int. Conf. on the Fundamentals of Tribology,* Massachusetts Institute of Technology Press, Cambridge, MA, 1987, p 469–476
8. S.L. Rice, The Role of Microstructure in the Impact Wear of Two Aluminium Alloys, *Wear,* Vol 54 (No. 2), 1987, p 291–301
9. S.L. Rice and S.F. Wayne, Wear of Two Titanium Alloys under Repetitive Compound Impact, *Wear,* Vol 61, 1980, p 69–76
10. S.L. Rice and R. Solecki, "Wear of Homogeneous and Composite Materials under Conditions of Repeated Normal and Sliding Impact," AFOSR Technical Report 1241, 1979
11. S.L. Rice, H. Nowotny, and S.L. Wayne, Formation of Subsurface Zones in Impact Wear, *ASLE Trans.,* Vol 24 (No. 2), 1981, p 264–268
12. S.L. Rice, H. Nowotny, and S.L. Wayne, Characteristics of Metallic Subsurface Zones in Sliding and Impact Wear, *Wear,* Vol 74, 1981, p 131–142
13. P.A. Engel, *Impact Wear of Materials,* Elsevier, Amsterdam, 1976
14. G.W. Stachowiak and A.W. Batchelor, *Engineering Tribology,* Butterworth Heinemann, Boston, 2001
15. R.S. Montgomery, The Mechanism of Percussive Wear of Tungsten Carbide Composites, *Wear,* Vol 12, 1968, p 309–329
16. E. Rabinowicz, Metal Transfer during Static Loading and Impacting, *Proc. Phys. Soc. B,* Vol 65, 1952, p 630–640
17. R.G. Bayer, P.A. Engel, and S.L. Sirico, Impact Wear Testing Machine, *Wear,* Vol 19, 1972, p 343–354
18. E.B. Iturbe, I.G. Greenfield, and T.W. Chow, Surface Layer Hardening of Polycrystalline Copper by Multiple Impact, *J. Mater. Sci.,* Vol 15, 1980, p 2331–2334
19. G. Laird, Repetitive- and Single-Blow Impact Testing of Wear Resistant Alloys, *J. Test. Eval.,* Vol 23 (No. 5), 1995, p 333–340
20. C.J. Studman and F.E. Field, A Repeated Impact Testing Machine, *Wear,* Vol 41, 1977, p 373–381
21. I.R. Sare, Repeated Impact-Abrasion of Ore-Crushing Hammers, *Wear,* Vol 87, 1983, p 202–225
22. P.A. Engel, H.C. Lee, and J.L. Zable, Dynamic Response of a Print Belt System, *IBM J. Res. Dev.,* Vol 23 (No. 4), 1979, p 403–410
23. S.L. Rice, S.F. Wayne, and H. Nowotny, Material Transport Phenomena in the Impact Wear of Titanium Alloys, *Wear,* Vol 61, 1980, p 215–226
24. S.L. Rice, H. Nowotny, and S.F. Wayne, The Role of Specimen Stiffness in Sliding and Impact Wear, *Wear,* Vol 77 (No. 1), 1982, p 13–28
25. Y. Yang, H. Fang, Y. Zheng, Z. Yang, and Z. Jiang, The Failure Models Induced by White Layers during Impact Wear, *Wear,* Vol 185, 1995, p 17–22
26. B. Zhang, Y. Liu, W. Shen, Y. Wang, X. Tang, and X. Wang, A Study on the Behaviour of Adiabatic Shear Bands in Impact Wear, *Wear,* Vol 198, 1996, p 287–292
27. N. P. Suh, The Delamination Theory of Wear, *Wear,* Vol 25, 1973, p 111–124
28. N.P. Suh, An Overview of the Delamination Theory of Wear, *Wear,* Vol 44, 1977, p 1–16
29. R.W. Fricke and C. Allen, Repetitive Impact-Wear of Steels, *Wear,* Vol 163, 1993, p 837–847
30. M. Lindroos, V. Ratia, M. Apostol, K. Valtonen, A. Laukkanen, W. Molnar, K. Holmberg, and V.-T. Kuokkala, The Effect of Impact Conditions on the Wear and Deformation Behavior of Wear Resistant Steels, *Wear,* Vol 328, 2015, p 197–205
31. H. Nowotny, S.L. Rice, and S.F. Wayne, Impact Wear of a Tool Steel, *Wear,* Vol 81 (No. 1), 1982, p 175–181
32. N. Saka, A. Eleiche, and N.P. Suh, Wear of Metals at High Sliding Speeds, *Wear,* Vol 44, 1977, p 109–126
33. S.L. Rice, H. Nowotny, and S.F. Wayne, Specimen Counterface Bulk Hardness Effects in Impact Wear of 17-4 PH Steel Pairs, *Wear,* Vol 103 (No. 2), 1985, p 175–185
34. T. Slatter, H. Taylor, R. Lewis, and P. King, The Influence of Laser Hardening on Wear in the Valve and Valve Seat Contact, *Wear,* Vol 267, 2009, p 797–806
35. S. Tianmin, H. Meng, and T.H. Yuen, Impact Wear Behavior of Laser Hardened Hypoeutectoid 2Cr13 Martensite Stainless Steel, *Wear,* Vol 255, 2003, p 444–455
36. T. Slatter, R. Lewis, and A.H. Jones, The Influence of Induction Hardening on the Impact Wear Resistance of Compacted Graphite Iron (CGI), *Wear,* Vol 270, 2011, p 302–311

37. T. Slatter, R. Lewis, and A.H. Jones, The Influence of Cryogenic Processing on Wear on the Impact Wear Resistance of Low Carbon Steel and Lamellar Graphite Cast Iron, *Wear,* Vol 271, 2011, p 1481–1489
38. M. Akhondizadeh, M.F. Mahani, M. Rezaeizadeh, and S. Mansouri, Experimental Investigation of the Impact Wear, *Mech. Ind.,* Vol 15, 2014, p 39–44
39. E. Rigaud and A. Le Bot, Influence of Incidence Angle on Wear Induced by Sliding Impacts, *Wear,* Vol 307, 2013, p 68–74
40. E.S. Zanoria and P.J. Blau, Effect of Incidence Angle on the Impact-Wear Behaviour of Silicon Nitride, *J. Am. Ceram. Soc.,* Vol 81 (No. 4), 1998, p 901–909
41. T. Ootani, N. Yahata, A. Fujiki, and A. Ehira, Impact Wear Characteristics of Engine Valve and Valve Seat Insert Materials at High Temperature (Impact Wear Tests of Austenitic Heat-Resistant Steel SUH36 against Fe-Base Sintered Alloy Using Plane Specimens), *Wear,* Vol 188, 1995, p 175–184
42. M.L.V. Ratia, K. Valtonen, M. Apostol, and V.-T. Kuokkala, Impact Behavior of Martensitic Steel at Low Temperatures, *Proceedings of the Nordic Symposium on Tribology* (Hämeenlinna, Finland), 2016
43. H. Nowotny, S.L. Rice, and S.F. Wayne, Characteristics of Wear Debris in Impact Sliding, *Wear,* Vol 68, 1981, p 159–167
44. S.R. Srinivasan and P.J. Blau, Effect of Relative Humidity on Repetitive Impact Behaviour of Machined Silicon Nitride, *J. Am. Ceram. Soc.,* Vol 77 (No. 3), 1994, p 683–688
45. E.S. Zanoria and P.J. Blau, Effects of Machined Surface Condition on the Repeated Impact Behaviour of Silicon Nitride, *Wear,* Vol 218, 1998, p 66–77
46. S.R. Srinivasan, P.J. Blau, and J.L. Bjerke, Effect of Machining Residual Stresses on the Repetitive Impact Behaviour of Silicon Nitride, *J. Mater. Res.,* Vol 10 (No. 1), 1995, p 95–100
47. R. Bantle and A. Matthews, Investigation into the Impact Wear Behaviour of Ceramic Coatings, *Surf. Coat. Technol.,* Vol 74–75, 1995, p 857–868
48. R.G. Bayer, Impact Wear of Elastomers, *Wear,* Vol 112, 1986, p 105–120
49. S.L. Rice, Reciprocating Impact Wear Testing Apparatus, *Wear,* Vol 45, 1977, p 85–95
50. R.G. Bayer and E. Sacher, The Effect of Voids on the Sliding Friction of Polyimide Film, *Wear,* Vol 37, 1976, p 15–20
51. G.E. Johnson, H.E. Bair, E.W. Anderson, and J.H. Daane, The Nature of Water in Polyethylene and Its Relationship to Dielectric Loss, *Proc. National Academy of Sciences National Research Council Conf. on Electrical Insulation and Dielectric Phenomena,* 1976
52. R.G. Bayer, P.A. Engel, and E. Sacher, Impact Wear Phenomena in Thin Polymer Films, *Wear,* Vol 32, 1975, p 181–194
53. P.J. Blau and T.A. Hanft, Quantitative Measurement of Repetitive Impact Damage on Ground Silicon Nitride Surfaces, *Tribol. Int.,* Vol 27 (No. 2), 1994, p 109–118
54. N.J. Mahoney, R.J. Grieve, and T. Ellis, A Simple Experimental Method for Studying the Impact Wear of Metals, *Wear,* Vol 98 (No. 1–3), 1984, p 79–87
55. P.A. Engel, Percussive Impact Wear, *Tribol. Int.,* Vol 11, 1978, p 169–176
56. K. Wellinger and H. Breckel, Kenngrossen und Verscheiss Beim Stoss Metallischer Werkstoffe (in German), *Wear,* Vol 13, 1969, p 257–281
57. E. Rabinowicz, *Friction and Wear of Materials,* John Wiley & Son, New York, 1995
58. R. Lewis and R.S. Dwyer-Joyce, "Design Tools for Predicting Inlet Valve Recession and Solving Valve Failure Problems," SAE Paper 2001-01-1987, presented at the SAE International Spring Fuel and Lubricants Meeting, May 7–9, 2001 (Orlando, FL), in SP-1624, 2001, p 105–114
59. M. Akhondizadeh, M.F. Mahani, M. Rezaeizadeh, and S. Mansouri, Propose a New Model for Prediction of the Impact Wear Using an Experimental Method, *J. Solid Mech.,* Vol 5, 2013, p 245–252
60. R. Lewis, R.S. Dwyer-Joyce, and G. Josey, Investigation of Wear Mechanisms Occurring in Passenger Car Diesel Engine Inlet Valves and Seat Inserts, *J. Fuels Lubr., Trans. SAE 1999,* 2000, p 610–618
61. R. Lewis, R.S. Dwyer-Joyce, G. Josey, Design and Development of a Bench Test-Rig for Investigating Diesel Engine Inlet Valve and Seat Wear, *Trans. Mech. Eng., Inst. Eng. Austral.,* Vol ME24 (No. 1), 2000, p 39–46
62. R. Lewis and R.S. Dwyer-Joyce, An Experimental Approach to Solving Combustion Engine Valve and Seat Wear Problems, *Proceedings of the 27th Leeds-Lyon Symposium on Tribology,* Elsevier Tribology Series No. 39, 2001, p 629–640
63. J.F. Archard, Contact and Rubbing of Flat Surfaces, *J. Appl. Phys.,* Vol 24 (No. 8), 1953, p 981–988